Published in final edited form as:

Oncogene. 2016 October 13; 35(41): 5412–5421. doi:10.1038/onc.2016.79.

RSK2 signals through stathmin to promote microtubule dynamics and tumor metastasis

GN Alesi[1], **L Jin**[1], **D Li**[1], **KR Magliocca**[2], **Y Kang**[3], **ZG Chen**[1], **DM Shin**[1], **FR Khuri**[1], and **S Kang**[1]

[1]Winship Cancer Institute, Department of Hematology and Medical Oncology, Emory University School of Medicine, Atlanta, GA, USA

[2]Department of Pathology and Laboratory Medicine, Emory University School of Medicine, Atlanta, GA, USA

[3]Department of Molecular Biology, Princeton University, Princeton, NJ, USA

Abstract

Metastasis is responsible for >90% of cancer-related deaths. Complex signaling in cancer cells orchestrates the progression from a primary to a metastatic cancer. However, the mechanisms of these cellular changes remain elusive. We previously demonstrated that p90 ribosomal S6 kinase 2 (RSK2) promotes tumor metastasis. Here we investigated the role of RSK2 in the regulation of microtubule dynamics and its potential implication in cancer cell invasion and tumor metastasis. Stable knockdown of RSK2 disrupted microtubule stability and decreased phosphorylation of stathmin, a microtubule-destabilizing protein, at serine 16 in metastatic human cancer cells. We found that RSK2 directly binds and phosphorylates stathmin at the leading edge of cancer cells. Phosphorylation of stathmin by RSK2 reduced stathmin-mediated microtubule depolymerization. Moreover, overexpression of phospho-mimetic mutant stathmin S16D significantly rescued the decreased invasive and metastatic potential mediated by RSK2 knockdown *in vitro* and *in vivo*. Furthermore, stathmin phosphorylation positively correlated with RSK2 expression and metastatic cancer progression in primary patient tumor samples. Our finding demonstrates that RSK2 directly phosphorylates stathmin and regulates microtubule polymerization to provide a pro-invasive and pro-metastatic advantage to cancer cells. Therefore, the RSK2–stathmin pathway represents a promising therapeutic target and a prognostic marker for metastatic human cancers.

Correspondence: Dr S Kang, Winship Cancer Institute, Department of Hematology and Medical Oncology, Emory University School of Medicine, 1365-C Clifton Road NE, Suite C3006, Atlanta, GA 30322, USA. smkang@emory.edu.

CONFLICT OF INTEREST

The authors declare no conflict of interest.

AUTHOR CONTRIBUTIONS

YK, ZGC, DMS and FRK provided critical reagents. LJ performed IHC staining and BLI study. KRM performed histopathological study. GNA and DL performed all the other experiments. GNA, LJ and SK designed the study and wrote the manuscript.

Supplementary Information accompanies this paper on the Oncogene website (http://www.nature.com/onc)

INTRODUCTION

Metastasis remains difficult to treat and therefore continues to be responsible for about 90% of human cancer deaths.[1,2] Cancer cell metastasis is a multi-stage process characterized by loss of cellular adhesion, increased motility and invasiveness, entry and survival in the circulation, exit into new tissue and eventual colonization at a distant site.[1,3,4] However, the molecular processes underlying these cellular changes remain elusive. Therefore, defining pro-metastatic signaling pathways is necessary to develop molecular therapies for metastasis and improve clinical outcomes.

Protein kinases are key mediators of extracellular and intracellular signaling and are often implicated in human cancer metastases. For example, AKT and ILK1 have important roles in breast cancer cell invasion and tumor metastasis.[5,6] We previously found that p90 ribosomal S6 kinase 2 (RSK2) signaling is commonly important in providing anoikis resistance, cell invasion and pro-metastatic signals in diverse metastatic human cancer cells, including lung, breast and head and neck cancer.[7–9] RSK2 belongs to the RSK serine/threonine kinase family and is a downstream substrate of extracellular signal–regulated kinase. RSKs are involved in various cellular processes, including gene expression, cell cycle and cell survival, by phosphorylating multiple signaling effectors, including cAMP response element-binding (CREB),[10] myelin transcription factor 1,[11] BAD and Bim,[12,13] respectively.[14–16]

Metastasis requires cell motility, which is partly driven by dynamic instability of microtubules.[17,18] Microtubules are protein filaments comprised of heterodimeric α−/β-tubulin subunits that dynamically switch between self-assembly and disassembly phases. This dynamic instability is largely regulated by stathmin (also known as STMN, oncoprotein 18, OP18, metablastin and p19).[18] Stathmin binds to the end of microtubules to sequester free tubulin and promote microtubule depolymerization, resulting in increased microtubule catastrophe and dynamics in cells.[19] Studies in sarcoma, colorectal, hepatoma, nasopharyngeal, breast cancer and gastric cancer cells report that stathmin expression positively correlates with metastatic potential.[20–24] Several transcription factors downstream of growth signaling pathways, including E2F, c-Jun, FoxM1 and CREB, are reported to increase stathmin expression in cancer cells.[25–28] Conversely, studies show that stathmin protein is downregulated in metastatic breast cancer.[29] Stathmin is also regulated at the posttranslational level via phosphorylation at N-terminal serines, S16, S25, S38 and S63. Phosphorylation is critical for inhibiting stathmin activity.[30–33] Increased phosphorylation of stathmin promotes dissociation from tubulin, which permits microtubule stabilization and polymerization.[33] Studies suggest a model of increasing stathmin phosphorylation by several pro-mitogenic kinases as the cell-cycle progresses to allow for proper spindle formation and mitosis.[34] Ca^{2+}/calmodulin-dependent protein kinases (CaMKs) are shown to phosphorylate stathmin at S16 in response to Ca^{2+} stimulation. In addition, activation of Rac/Cdc42 proteins induces p21-activated kinase 1 (PAK1)-dependent stathmin phosphorylation.[30,31,34] A clinically relevant point mutation in the N-terminal regulatory region of stathmin has been found to greatly enhance its microtubule sequestering ability, thereby causing aggressive invasion in comparison to its overexpressed wild-type (WT) counterpart.[20,35,36]

These findings suggest that stathmin has an important role in many types of cancers and may therefore be a promising target for cancer therapy.[34] Although stathmin activity is highly regulated via phosphorylation on N-terminal serine residues, the regulation of stathmin phosphorylation in metastatic cancers is not fully understood. Here we report that RSK2 signals through stathmin to regulate cytoskeleton stability and promotes cancer cell invasion and tumor metastasis in human cancers.

RESULTS

RNAi-mediated RSK2 knockdown attenuates microtubule polymerization in metastatic cancer cells

To better understand the role of RSK2 in pro-metastatic signaling, we tested the effect of blocking RSK2 on microtubule dynamics. Targeted downregulation of RSK2 using two different short hairpin RNA (shRNA) clones resulted in significant reduction of microtubule polymerization in metastatic lung cancer A549 and head and neck squamous cell carcinoma (HNSCC) 212LN cell lines as measured by microtubule sedimentation assay (Figure 1a), immunofluorescence staining (Figure 1b) and fluorescence-based quantitative whole-cell microtubule analysis (Figure 1c). Immunofluorescence imaging revealed that tubulin was evenly distributed as bundles in control A549 cells transduced with an empty vector, whereas it was predominantly depolymerized in cells with stable RSK2 knockdown (Figure 1b). Moreover, overexpression of shRNA-resistant human constitutively active (CA; Y707A) RSK2, but not kinase dead (KD; Y707A/K100A) RSK2, rescued the tubulin depolymerization induced by RSK2 knockdown (Figure 1d). These data suggest that RSK2 promotes microtubule polymerization in metastatic cancer cells in a kinase-dependent manner.

Targeted downregulation of RSK2 attenuates stathmin phosphorylation at serine 16

Dysregulation of microtubule formation and stability in cancer can lead to increased cell motility and metastasis. Microtubule dynamics are mainly modulated by stathmin. Stathmin binds tubulin heterodimers and destabilizes microtubules. Phosphorylation of stathmin at N-terminal serines inhibits stathmin activity and is crucial for promoting microtubule stability. To demonstrate whether RSK2 promotes microtubule polymerization through phosphorylation of stathmin, the phosphorylation levels of stathmin at S16, S25, S38 and S63 were determined in diverse metastatic cancer cell lines with RSK2 knockdown. We found that stable knockdown of RSK2 using two different shRNA clones resulted in decreased phosphorylation of stathmin at S16 in lung cancer A549, HNSCC 212LN and breast cancer SKBR3 cell lines (Figure 2a). Conversely, the phosphorylation levels at other N-terminal serines of stathmin, including S25, S38 and S63 were not altered upon RSK2 knockdown (Figure 2b). Moreover, RSK2 knockdown did not affect activity of the known upstream kinases of stathmin, including CaMKII and PAK1, in A549, 212LN and SKBR3 cells (Figure 2c). The activity of CaMKII and PAK1 was assessed by autophosphorylation at T286 and S199/S204, respectively. These data suggest that RSK2 contributes to stathmin phosphorylation at S16, and this is not mediated through the known upstream kinases, CaMKII or PAK1.

RSK2 associates with and phosphorylates stathmin at serine 16

Next we tested whether RSK2 directly phosphorylates stathmin at S16. Purified recombinant stathmin variants, WT and phospho-deficient mutants S16A and S31A, were incubated with recombinant active RSK2 in an *in vitro* kinase assay. As shown in Figure 3a, both WT and S31A stathmin were phosphorylated at S16 by RSK2, whereas S16 phosphorylation was not observed for the stathmin S16A mutant. The structural properties of the recombinant stathmin variants were evaluated by proteolytic digestion (Figure 3b). Purified recombinant flag-tagged stathmin WT, S16A and S31A were incubated with chymotrypsin. The digestion patterns of the mutant proteins and WT were similar, suggesting that the global structure of mutant proteins was not altered and the observed phosphorylation patterns were not caused by a structural change.

To further investigate the RSK2-dependent phosphorylation of stathmin in cells, we tested whether RSK2 interacts with stathmin. First, we found that stathmin predominantly colocalizes with RSK2 in the cytosol (Figures 3c and d). Binding was confirmed by co-immunoprecipitation using lysates of 293T cells expressing flag-tagged stathmin and glutathione *S*-transferase (GST)-fused RSK2. Flag-stathmin was detected in the bead-bound GST-RSK2 sample but not the GST control sample, suggesting that RSK2 interacts with stathmin in cells (Figure 3e). Moreover, endogenous RSK2 and stathmin interact in A549 and 212LN cancer cells (Figure 3f).

In addition, we performed immunofluorescent staining to determine the phosphorylation status of stathmin in A549 cells with or without RSK2 knockdown (Figure 3g). Stathmin phosphorylation at S16 was markedly reduced with stable RSK2 knockdown. Phosphorylated stathmin largely co-exists with α-tubulin in the cytoplasm. Interestingly, a significant portion of phosphorylated stathmin was located at the leading edge of cancer cells as indicated by arrows (Figure 3g), whereas the phosphorylated form was markedly reduced in A549 cells with stable RSK2 knockdown. These data together suggest that RSK2 binds and phosphorylates stathmin in part at the leading edge of cancer cells.

RSK2-dependent phosphorylation of stathmin attenuates microtubule-destabilizing activity of stathmin

To further investigate the role of RSK2-dependent phosphorylation in stathmin activation, we performed a series of coupled *in vitro* kinase assays and microtubule polymerization assays (Figures 4a–e). Stathmin was phosphorylated via an *in vitro* RSK2 kinase assay and was subsequently incubated with purified bovine tubulin for polymerization. Polymerized tubulin was assessed using three different assays: microtubule sedimentation (Figures 4a–c), immunofluorescence staining (Figure 4d), and fluorimetry-based tubulin polymerization (Figure 4e). RSK2 alone did not affect tubulin polymerization (Figures 4b–e, left panels). Incubation with stathmin markedly reduced tubulin polymer formation, whereas phosphorylation of stathmin by RSK2 significantly attenuated stathmin activity and partially restored tubulin polymerization *in vitro* (Figures 4b–e, right panels). Moreover, incubation of stathmin with recombinant inactive RSK2 (KD RSK2) *in vitro* (Figure 4e) or overexpression of KD RSK2 in RSK2 knockdown cells (Figure 4f) did not alter tubulin depolymerizing activity of stathmin, suggesting that RSK2-mediated regulation of stathmin

is phosphorylation dependent. Furthermore, co-overexpression of CA RSK2 and WT stathmin, but not S16A stathmin, restored the decreased tubulin polymerization in cells with RSK2 knockdown (Figure 4f). These data suggest that RSK2 promotes tubulin polymerization by phosphorylating stathmin at serine16 and consequently inhibiting stathmin activity.

Phosphorylation of stathmin by RSK2 is required for RSK2-driven cancer cell invasion and tumor metastasis

To demonstrate whether stathmin, as a downstream phosphorylation target of RSK2, contributes to RSK2-dependent pro-invasive and pro-metastatic signals in cancer cells, metastatic cancer cell lines with stable knockdown of RSK2 and forced expression of phospho-mimetic or -deficient mutants of stathmin were generated and examined for invasive and metastatic potential *in vitro* and *in vivo* (Figure 5 and Supplementary Figure S1). Silencing RSK2 using two different shRNA clones significantly attenuated the invasive capacity of metastatic A549 and 212LN cells, whereas expression of the stathmin phospho-mimetic mutant S16D, but not the phospho-deficient mutant S16A, significantly rescued the decrease in cell invasion owing to RSK2 knockdown (Figure 5a and Supplementary Figure S1A).

Next we tested whether phosphorylation of stathmin by RSK2 is required to promote tumor metastasis *in vivo* using a xenograft mouse model. Luciferase-labeled A549 cells with stable RSK2 knockdown and S16A or S16D stathmin overexpression (Figure 5b and Supplementary Figure S1B) were injected intravenously into nude mice and subjected to bioluminescent imaging (BLI).[37] The group injected with RSK2 knockdown cells showed significantly attenuated lung metastasis compared with the control group injected with cells harboring empty vectors (Figure 5c and Supplementary Figure S1C). Overexpression of the stathmin phospho-mimetic mutant S16D, but not the phospho-deficient mutant S16A, significantly rescued the decrease in metastatic potential caused by RSK2 knockdown *in vivo* (Figure 5c and Supplementary Figure S1C). Taken together, these analyses show that RSK2 signals through stathmin by phosphorylation at serine 16 to promote cancer cell invasion and tumor metastasis.

Stathmin phosphorylation and RSK2 expression patterns correlate in primary human tumor tissue samples from lung cancer patients To further explore the clinical importance of the RSK2–stathmin signaling axis in tumor metastasis, we examined whether stathmin phosphorylation positively correlates with metastatic cancer progression and with RSK2 expression in primary human lung cancer tissue samples. Tissue microarray containing 40 cases of primary lung cancer with matched lymph node metastasis was used for immunohistochemistry (IHC) to detect phospho-S16 stathmin and RSK2 expression (Figure 6). As shown in Figure 6a, RSK2 and phospho-stathmin S16 staining intensity in the tumor cells was scored on a scale from 0 to 3+ (Figure 6a). The IHC studies demonstrate that the levels of RSK2 expression and stathmin phosphorylation positively correlate with metastatic progression. Both RSK2 and phospho-stathmin staining levels were significantly higher in tumor tissue samples from metastatic lymph nodes compared with the paired primary tumor specimens (Figure 6b). Furthermore, we found a positive correlation between staining scores

of RSK2 and phospho-S16 stathmin (Figure 6c). These data together support a functional cooperation between RSK2 and stathmin in tumor metastasis of human lung cancer.

DISCUSSION

Our data support that RSK2 signals through stathmin and inhibits its microtubule-destabilizing activity. We provide evidence that targeting RSK2 reduces the invasive and metastatic potential of cancer cells, while overexpression of the phospho-mimetic mutant S16D but not the phospho-deficient mutant S16A form of stathmin can partially rescue the reduced cancer cell invasion and tumor metastasis owing to the attenuation of RSK2 *in vitro* and *in vivo*. Clinically, we observed that the phosphorylation level of stathmin at S16 positively correlates with RSK2 expression and metastatic tumor progression in patient tumor tissues. These findings link RSK2 signaling to microtubule dynamics through stathmin providing a pro-invasive and pro-metastatic advantage to human cancers. Therefore, the RSK2–stathmin pathway may represent a promising prognostic marker and a therapeutic target for the treatment of metastatic human cancers.

Stathmin is a promising anticancer target owing to its critical role in microtubule dynamics and cell migration. Our study supports that stathmin serves as a signaling effector of RSK2 and contributes to RSK2-mediated microtubule polymerization. We previously reported Hsp27 as an alternative RSK2 phosphorylation target. RSK2 phosphorylates Hsp27 at S78 and S82 to promote actin filament formation and cell invasion.[8] In addition, we reported that the RSK2–CREB pathway promotes filopodia formation by upregulating Fascin-1, a major bundling protein in filopodia.[9] Together, our studies suggest that RSK2 functions as a signal integrator to modulate dynamics of the cytoskeleton, including microtubules, microfilaments, and filopodia, via a network of phosphorylation targets and transcription targets of RSK2 in both transcription-independent and -dependent manners. Further research is warranted to explore the coordinated potential between different RSK2 targets, which may ultimately provide RSK2-dependent antianoikis, pro-migratory, pro-invasive and pro-metastatic signaling in human cancers.

RNAi-mediated downregulation of RSK2 partially decreased the polymerized tubulin biomass in cells. Although RSK2 significantly affected cellular tubulin polymerization, RSK2 likely acts in tandem with other critical signaling factors and contribute to microtubule dynamics in cancer cells. It is worth considering that the phosphorylation of stathmin by RSK2 partially rescued the microtubule-depolymerizing activity of stathmin *in vitro*. This indicates that the phosphorylation of stathmin at S16 could be modulated through not only RSK2 but also other protein kinases, including PKA, CaMKII, PAK1 and Aurora.[34] In addition, phosphatases such as PP1, PP2A or PP2B could be involved in the dephosphorylation of stathmin.[38,39] Nevertheless, phosphorylation of stathmin at S16 was significantly diminished upon RSK2 knockdown in cancer cells, indicating that RSK2 is the predominant upstream stathmin kinase in the cancer cells we tested. Further comprehensive comparison using additional cell lines and cancer types would be required to determine the contribution of kinases and phosphatases to stathmin activation in distinct cancer cells.

Although serine phosphorylation at the N-terminal residues is the most commonly known mechanism of stathmin modulation, the activity of stathmin is also controlled by protein sequestration. Signal transducer and activator of transcription 3 and the cyclin-dependent kinase inhibitor $p27^{Kip1}$ bind to stathmin and block its ability to sequester free α−/β-tubulin dimers from microtubules. We demonstrated that RSK2 not only phosphorylates stathmin but also associates with stathmin in cells. In addition, we found that inactive RSK2 does not alter tubulin polymerization and stathmin activity *in vitro* and *in vivo*. Therefore, RSK2 likely interacts with stathmin to modulate cell motility in a phosphorylation-dependent manner.

Finally, stathmin contributes to several biological processes, including control of cell cycle progression, apoptosis and cell migration. Stathmin is a target of apoptosis-signaling-regulating kinase 1 (ASK1)–p38.[40] We recently reported that RSK2 signals through ASK1 to mediate resistance to anoikis, an apoptotic process induced by loss of cell adhesion.[7] Therefore, stathmin may not only contribute to RSK2-dependent pro-migratory potential but also to anoikis resistance through ASK1 in cancer cells. The comprehensive characterization of RSK2 and its essential downstream signaling effectors will provide critical information to advance our understanding of the signaling mechanisms underlying metastatic progression.

MATERIALS AND METHODS

Reagents

ShRNA constructs for RSK2, sense strand GCCTGAAGATACATTCTATTT for clone #1 and CGCTGAGAATGGACAGCAAAT for clone #2, were purchased from Dharmacon, GE Healthcare Life Sciences (Lafeyette, CO, USA). The RSK2 constructs, pDEST27-RSK2 and pLHCX-mycRSK2 variants, have been previously described.[7,41] Human RSK2 CA mutant Y707A or a KD mutant Y707A/K100A,[42] which are resistant to RSK2 shRNA by introducing silent mutations in the shRNA target sequence, were generated using QuikChange-XL Site-directed Mutagenesis Kit (Stratagene, San Diego, CA, USA). The image clone for stathmin1 (GenBank accession number BC082228, clone ID 2822803) was purchased from GE Healthcare Life Sciences. Flag tag was added to stathmin by PCR and subcloned into the pLHCX-Gateway vector. A549 and SKBR3 cells were from American Type Culture Collection (Manassas, VA, USA). 212LN cells were obtained as described previously.[8] A549-Luc-GFP cell line was generated from A549 cells using a bioluminescent and fluorescent imaging vector.[37] Purified recombinant active and inactive RSK2 were obtained from Invitrogen. Purified bovine tubulin, rhodamine-labeled tubulin and *In Vitro* Tubulin Polymerization Assay Kit were from Cytoskeleton, Inc. (Denver, CO, USA).

Antibodies

Antibodies against β-actin (A1978/AC-15), flag (F7425), GST (G1160/GST-2) and α-tubulin conjugated with FITC (fluorescein isothiocyanate; F2168/DM1A) were from Sigma Aldrich (St Louis, MO, USA). Anti-phospho-S16 stathmin (3353), phospho-S38 stathmin (4191/D19H10), stathmin (3352), phospho-T286 CaMKII (3361), pan CaMKII (4436/D11A10), phospho-PAK1/2 S199/S204 (2605) and PAK1 (2602) antibodies were purchased from Cell Signaling Technology Inc. (Danvers, MA, USA). Antibodies against tubulin

(sc23948/B-5-1-2), RSK2 (sc9986/E-1) and phospho-S16 stathmin (sc12948-R) were from Santa Cruz Biotechnology (Dallas, TX, USA). Anti-phospho-S16 stathmin antibody (ab47328) for immunohistochemistry and western blotting, stathmin (ab52906) for immunoprecipitation and western blotting, phospho-S25 stathmin (ab62336/EP2124Y) and phospho-S63 stathmin (ab76583/EPR1574) antibodies were obtained from Abcam (Cambridge, MA, USA). Anti-RSK2 antibody (NB110-57472/Y82) for immunohistochemistry was from Novus Biologicals (Littleton, CO, USA).

Cell culture

A549 cells were cultured in RPMI 1640 medium with 10% fetal bovine serum (FBS). 212LN cells were cultured in Dulbecco Modified Eagle Medium (DMEM)/Ham's F-12 50/50 mix medium in the presence of 10% FBS. 293T and SKBR3 cells were cultured in DMEM with 10% FBS. Cell lines with stable RSK2 knockdown and overexpression of flag-tagged stathmin variants were obtained by lentiviral and retroviral infection as previously described.[43]

Microtubule sedimentation assay

The level of polymerized and depolymerized forms of tubulin in cells were measured using a modification of the procedure that was previously described.[29] In brief, equal numbers of cells with or without RSK2 knockdown were lysed in the presence of 1 mg/ml paclitaxel. The cell lysates were centrifuged at 12 000 *g* for 10 min. The tubulin contents in the pellet and supernatant were analyzed by SDS–PAGE (sodium dodecyl sulfate-polyacrylamide gel electrophoresis) followed by immunoblotting with anti-tubulin antibody. The fraction of tubulin in the polymerized state was calculated by taking the ratio of tubulin in the pellet divided by the sum of the ratios of tubulin in the pellet and its corresponding supernatant.

FACS (fluorescence-activated cell sorting)-based whole-cell analysis of tubulin polymerization

Polymerized tubulin in cells was quantified as previously described with slight modifications.[44] Briefly, 3×10^5 cells were fixed for 10 min with 1 ml of 0.5% glutaraldehyde in Microtubule Stabilizing Buffer (80 mM PIPES, 1 mM $MgCl_2$, 5 mM EDTA and 0.5% Triton X-100, pH 6.8). In all, 0.7 ml of 1 mg/ml $BaBH_4$ was added and cells were pelleted by centrifugation at 1000 *g* for 10 min. The collected cells were incubated with 50 μg/ml RNase A for 12 h in Antibody Diluting Buffer (phosphate-buffered saline (PBS), 0.2% Triton X-100, 2% BSA and 0.1% NaN_3) followed by staining with anti-α-tubulin-FITC antibody (1:250) for 3 h. The samples were diluted in 0.5 ml of PBS containing 50 μg/ml propidium iodide and analyzed by flow cytometry.

In vitro microtubule-polymerization assay

Recombinant stathmin (6.4 μg) and/or RSK2 (1 μg) were mixed into 100 μl of tubulin polymerization buffer (80 mM PIPES, 0.5 mM EGTA, 2 mM $MgCl_2$, 1 mM GTP, 3.75% glycerol, pH 6.9) after *in vitro* RSK2 kinase assay with purified tubulin (0.5 mg/ml) and incubated for 1 h at 37 °C. Samples were centrifuged for 20 min at 40 000 r.p.m., 37 °C. The amount of microtubules in the pellet and supernatant were analyzed by SDS–PAGE and

Coomassie blue staining. Fluorescence studies were performed as previously described.[45] In brief, 2 mg/ml tubulin was polymerized with rhodamine-labeled tubulin in a 4:1 ratio at 37 °C for 60 min. Microtubules were spotted on a glass slide with mounting solution. Images were collected on Leica SP8 confocal microscope (Leica Microsystems GmbH, Wetzlar, Germany). For the fluorimetry-based tubulin-polymerization assay, microtubule assembly was measured using a Tubulin Polymerization Assay Kit (Cytoskeleton, Inc.) according to the manufacturer's instructions.

In vitro RSK2 kinase assay

Protein purification and proteolytic digestion were performed as previously described.[41] Purified recombinant flag-tagged stathmin WT, S16A and S31A were incubated with recombinant active RSK2 in 20 mM MOPS, 1 mM DTT, 5 mM EGTA, 1 mM Na_3VO_4, 25 mM β-glycerol phosphate and 15 mM $MgCl_2$ along with 10 mM MgAc and 0.1 mM ATP for 30 min at 30 °C. Phosphorylation of stathmin at serine 16 was detected by phospho-Ser16 stathmin-specific antibody.

Immunofluorescence staining

A549 cells were seeded on coverslips and fixed in PHEMO buffer (68 mM PIPES, 25 mM HEPES, 15 mM EGTA and 3 mM $MgCl_2$, 3.7% formaldehyde, 0.05% glutaraldehyde, 0.5% Triton X-100). Cells were blocked in 10% goat serum and then stained with anti-tubulin antibody and anti-phospho S16 stathmin antibody followed by Alexa Fluor 633-conjugated anti-mouse IgG antibody and Alexa 488-conjugated anti-rabbit IgG antibody, respectively. The coverslips were washed, mounted and imaged on a Zeiss LSM 510 META confocal microscope (Carl Zeiss, Oberkochen, Germany).

In vitro cell invasion assay

Transwell inserts with 8-μm pores (BD Biosciences, San Jose, CA, USA) were coated with Matrigel (BD Biosciences). Approximately, 4×10^4 cells were seeded on Matrigel-coated upper chambers with 0.3 ml serum-free media, and 0.5 ml of medium with 10% FBS was placed in the lower wells. The invaded cells were fixed and stained in 25% methanol and 0.5% crystal violet after 48-h incubation. Proliferation was determined by using the Celltiter96AQ_{ueous} One Solution Proliferation Kit (Promega, Madison, WI, USA). Invasion was assessed as the number of cells that had invaded through the membrane normalized by the proliferation.

In vivo xenograft assay and BLI

Animal experiments were performed according to the protocols approved by the Institutional Animal Care and Use Committee of Emory University. Nude mice (athymic nu/nu, female, 4–6-week old, Harlan, Indianapolis, IN, USA) were intravenously injected with 2.5×10^6 of A549-luc-GFP cells with RSK2 knockdown and expression of stathmin mutants. Metastasis was monitored by BLI analysis as described.[37] In brief, xenograft mice were administered 75 mg/kg of D-luciferin intraperitoneally 3 min before the BLI imaging (Perkin Elmer, Waltham, MA, USA, 15 mg/ml solution in sterile PBS). BLI images were acquired by using

Xenogen IVIS system coupled to Living Image acquisition and analysis software (Perkin Elmer).

Tissue microarray analysis

Approval of use of human specimens was given by the Emory University Institutional Review Board. All of the clinical samples were collected with informed consent under Health Insurance Portability and Accountability Act approved protocols.

Paraffin-embedded lung cancer with matched lymph node metastasis tissue array (LC814) was obtained from US Biomax, Inc. (Rockville, MD, USA). IHC analysis of RSK2 expression and stathmin phosphorylation was performed using tissue array samples as previously described.[46] In brief, human tissue sections were incubated in 3% hydrogen peroxide after deparaffinization and rehydration. Antigen retrieval was achieved by microwaving the sections in 100 mM Tris (pH 10.0) and 10 mM sodium citrate (pH 6.0) for RSK2 and phospho-stathmin S16 staining, respectively. The slides were subsequently blocked with 2.5% horse serum and avidin–biotin complex system (Vector Laboratories, Burlingame, CA, USA). The primary antibodies, anti-RSK2 antibody and anti-phospho-stathmin S16 antibody, were applied at a dilution of 1:100. Detection was achieved with 3,3′-diaminobenzidine and counterstained with hematoxylin. IHC staining results were scored as 0 for no staining, 1+ for weak staining, 2+ for moderate staining and 3+ for strong staining.

Statistics

Statistical analysis was performed using GraphPad Prism 6.0 (GraphPad Software, La Jolla, CA, USA). Data shown as images are from one representative experiment of multiple experiments. Data with error bars represent mean ± s.e.m. for Figures 5c and 6b and Supplementary Figure S1C and mean ± s.d. for all the other figures. Statistical analysis of significance was based on chi-square test for Figure 6c and Student's *t*-test for all the other figures.

Supplementary Material

Refer to Web version on PubMed Central for supplementary material.

Acknowledgments

We acknowledge Dr Anthea Hammond for editorial assistance. We thank the shared resources facilities of the Winship Cancer Institute and the Integrated Cellular Imaging Core of Emory University. We also acknowledge and thank Dr Shi-Yong Sun for his insightful scientific input in the development of this work. This work was supported in part by NIH grants R01 CA175316 (to SK), F31 CA183365 (to GNA) and ACS grant RSG-11-081-01 (to SK). GNA is an NIH predoctoral fellow. FRK and SK are Georgia Cancer Coalition Scholars. SK is a Robbins Scholar and an American Cancer Society Basic Research Scholar.

References

1. Fidler IJ. The pathogenesis of cancer metastasis: the 'seed and soil' hypothesis revisited. Nat Rev Cancer. 2003; 3:453–458. [PubMed: 12778135]
2. Nguyen DX, Massague J. Genetic determinants of cancer metastasis. Nat Rev Genet. 2007; 8:341–352. [PubMed: 17440531]

3. Gupta GP, Massague J. Cancer metastasis: building a framework. Cell. 2006; 127:679–695. [PubMed: 17110329]
4. Sahai E. Mechanisms of cancer cell invasion. Curr Opin Genet Dev. 2005; 15:87–96. [PubMed: 15661538]
5. Li Y, Wang JP, Santen RJ, Kim TH, Park H, Fan P, et al. Estrogen stimulation of cell migration involves multiple signaling pathway interactions. Endocrinology. 2010; 151:5146–5156. [PubMed: 20861240]
6. Persad S, Dedhar S. The role of integrin-linked kinase (ILK) in cancer progression. Cancer Metastasis Rev. 2003; 22:375–384. [PubMed: 12884912]
7. Jin L, Li D, Lee JS, Elf S, Alesi GN, Fan J, et al. p90 RSK2 mediates antianoikis signals by both transcription-dependent and -independent mechanisms. Mol Cell Biol. 2013; 33:2574–2585. [PubMed: 23608533]
8. Kang S, Elf S, Lythgoe K, Hitosugi T, Taunton J, Zhou W, et al. p90 ribosomal S6 kinase 2 promotes invasion and metastasis of human head and neck squamous cell carcinoma cells. J Clin Invest. 2010; 120:1165–1177. [PubMed: 20234090]
9. Li D, Jin L, Alesi GN, Kim YM, Fan J, Seo JH, et al. The prometastatic ribosomal S6 kinase 2-cAMP response element-binding protein (RSK2-CREB) signaling pathway up-regulates the actin-binding protein fascin-1 to promote tumor metastasis. J Biol Chem. 2013; 288:32528–32538. [PubMed: 24085294]
10. Buck M, Poli V, Hunter T, Chojkier M. C/EBPbeta phosphorylation by RSK creates a functional XEXD caspase inhibitory box critical for cell survival. Mol Cell. 2001; 8:807–816. [PubMed: 11684016]
11. Palmer A, Gavin AC, Nebreda AR. A link between MAP kinase and p34(cdc2)/cyclin B during oocyte maturation: p90(rsk) phosphorylates and inactivates the p34(cdc2) inhibitory kinase Myt1. EMBO J. 1998; 17:5037–5047. [PubMed: 9724639]
12. Shimamura A, Ballif BA, Richards SA, Blenis J. Rsk1 mediates a MEK-MAP kinase cell survival signal. Curr Biol. 2000; 10:127–135. [PubMed: 10679322]
13. Dehan E, Bassermann F, Guardavaccaro D, Vasiliver-Shamis G, Cohen M, Lowes KN, et al. betaTrCP- and Rsk1/2-mediated degradation of BimEL inhibits apoptosis. Mol Cell. 2009; 33:109–116. [PubMed: 19150432]
14. Blenis J. Signal transduction via the MAP kinases: proceed at your own RSK. Proc Natl Acad Sci USA. 1993; 90:5889–5892. [PubMed: 8392180]
15. Frodin M, Gammeltoft S. Role and regulation of 90 kDa ribosomal S6 kinase (RSK) in signal transduction. Mol Cell Endocrinol. 1999; 151:65–77. [PubMed: 10411321]
16. Anjum R, Blenis J. The RSK family of kinases: emerging roles in cellular signalling. Nat Rev Mol Cell Biol. 2008; 9:747–758. [PubMed: 18813292]
17. Schoumacher M, Goldman RD, Louvard D, Vignjevic DM. Actin, microtubules, and vimentin intermediate filaments cooperate for elongation of invadopodia. J Cell Biol. 2010; 189:541–556. [PubMed: 20421424]
18. Desai A, Mitchison TJ. Microtubule polymerization dynamics. Annu Rev Cell Dev Biol. 1997; 13:83–117. [PubMed: 9442869]
19. Belmont LD, Mitchison TJ. Identification of a protein that interacts with tubulin dimers and increases the catastrophe rate of microtubules. Cell. 1996; 84:623–631. [PubMed: 8598048]
20. Belletti B, Nicoloso MS, Schiappacassi M, Berton S, Lovat F, Wolf K, et al. Stathmin activity influences sarcoma cell shape, motility, and metastatic potential. Mol Biol Cell. 2008; 19:2003–2013. [PubMed: 18305103]
21. Tan HT, Wu W, Ng YZ, Zhang X, Yan B, Ong CW, et al. Proteomic analysis of colorectal cancer metastasis: stathmin-1 revealed as a player in cancer cell migration and prognostic marker. J Proteome Res. 2012; 11:1433–1445. [PubMed: 22181002]
22. Hsieh SY, Huang SF, Yu MC, Yeh TS, Chen TC, Lin YJ, et al. Stathmin1 overexpression associated with polyploidy, tumor-cell invasion, early recurrence, and poor prognosis in human hepatoma. Mol Carcinog. 2010; 49:476–487. [PubMed: 20232364]

23. Cheng AL, Huang WG, Chen ZC, Peng F, Zhang PF, Li MY, et al. Identification of novel nasopharyngeal carcinoma biomarkers by laser capture microdissection and proteomic analysis. Clin Cancer Res. 2008; 14:435–445. [PubMed: 18223218]
24. Jeon TY, Han ME, Lee YW, Lee YS, Kim GH, Song GA, et al. Overexpression of stathmin1 in the diffuse type of gastric cancer and its roles in proliferation and migration of gastric cancer cells. Br J Cancer. 2010; 102:710–718. [PubMed: 20087351]
25. Polzin RG, Benlhabib H, Trepel J, Herrera JE. E2F sites in the Op18 promoter are required for high level of expression in the human prostate carcinoma cell line PC-3-M. Gene. 2004; 341:209–218. [PubMed: 15474303]
26. Kinoshita I, Leaner V, Katabami M, Manzano RG, Dent P, Sabichi A, et al. Identification of cJun-responsive genes in Rat-1a cells using multiple techniques: increased expression of stathmin is necessary for cJun-mediated anchorage-independent growth. Oncogene. 2003; 22:2710–2722. [PubMed: 12743595]
27. Carr JR, Park HJ, Wang Z, Kiefer MM, Raychaudhuri P. FoxM1 mediates resistance to herceptin and paclitaxel. Cancer Res. 2010; 70:5054–5063. [PubMed: 20530690]
28. San-Marina S, Han Y, Liu J, Minden MD. Suspected leukemia oncoproteins CREB1 and LYL1 regulate Op18/STMN1 expression. Biochim Biophys Acta. 2012; 1819:1164–1172. [PubMed: 23000483]
29. Li N, Jiang P, Du W, Wu Z, Li C, Qiao M, et al. Siva1 suppresses epithelial-mesenchymal transition and metastasis of tumor cells by inhibiting stathmin and stabilizing microtubules. Proc Natl Acad Sci USA. 2011; 108:12851–12856. [PubMed: 21768358]
30. Daub H, Gevaert K, Vandekerckhove J, Sobel A, Hall A. Rac/Cdc42 and p65PAK regulate the microtubule-destabilizing protein stathmin through phosphorylation at serine 16. J Biol Chem. 2001; 276:1677–1680. [PubMed: 11058583]
31. Marklund U, Larsson N, Brattsand G, Osterman O, Chatila TA, Gullberg M. Serine 16 of oncoprotein 18 is a major cytosolic target for the Ca2+/calmodulin-dependent kinase-Gr. Eur J Biochem. 1994; 225:53–60. [PubMed: 7925472]
32. Beretta L, Dobransky T, Sobel A. Multiple phosphorylation of stathmin. Identification of four sites phosphorylated in intact cells and in vitro by cyclic AMP-dependent protein kinase and p34cdc2. J Biol Chem. 1993; 268:20076–20084. [PubMed: 8376365]
33. Cassimeris L. The oncoprotein 18/stathmin family of microtubule destabilizers. Curr Opin Cell Biol. 2002; 14:18–24. [PubMed: 11792540]
34. Belletti B, Baldassarre G. Stathmin: a protein with many tasks. New biomarker and potential target in cancer. Expert Opin Ther Targets. 2011; 15:1249–1266. [PubMed: 21978024]
35. Misek DE, Chang CL, Kuick R, Hinderer R, Giordano TJ, Beer DG, et al. Transforming properties of a Q18–>E mutation of the microtubule regulator Op18. Cancer Cell. 2002; 2:217–228. [PubMed: 12242154]
36. Holmfeldt P, Brannstrom K, Stenmark S, Gullberg M. Aneugenic activity of Op18/stathmin is potentiated by the somatic Q18–>e mutation in leukemic cells. Mol Biol Cell. 2006; 17:2921–2930. [PubMed: 16624860]
37. Kang Y, He W, Tulley S, Gupta GP, Serganova I, Chen CR, et al. Breast cancer bone metastasis mediated by the Smad tumor suppressor pathway. Proc Natl Acad Sci USA. 2005; 102:13909–13914. [PubMed: 16172383]
38. Tournebize R, Andersen SS, Verde F, Doree M, Karsenti E, Hyman AA. Distinct roles of PP1 and PP2A-like phosphatases in control of microtubule dynamics during mitosis. EMBO J. 1997; 16:5537–5549. [PubMed: 9312013]
39. Mistry SJ, Li HC, Atweh GF. Role for protein phosphatases in the cell-cycle-regulated phosphorylation of stathmin. Biochem J. 1998; 334:23–29. [PubMed: 9693097]
40. Mizumura K, Takeda K, Hashimoto S, Horie T, Ichijo H. Identification of Op18/stathmin as a potential target of ASK1-p38 MAP kinase cascade. J Cell Physiol. 2006; 206:363–370. [PubMed: 16110469]
41. Kang S, Dong S, Gu TL, Guo A, Cohen MS, Lonial S, et al. FGFR3 activates RSK2 to mediate hematopoietic transformation through tyrosine phosphorylation of RSK2 and activation of the MEK/ERK pathway. Cancer Cell. 2007; 12:201–214. [PubMed: 17785202]

42. Clark DE, Poteet-Smith CE, Smith JA, Lannigan DA. Rsk2 allosterically activates estrogen receptor alpha by docking to the hormone-binding domain. EMBO J. 2001; 20:3484–3494. [PubMed: 11432835]

43. Hitosugi T, Fan J, Chung TW, Lythgoe K, Wang X, Xie J, et al. Tyrosine phosphorylation of mitochondrial pyruvate dehydrogenase kinase 1 is important for cancer metabolism. Mol Cell. 2011; 44:864–877. [PubMed: 22195962]

44. Morrison KC, Hergenrother PJ. Whole cell microtubule analysis by flow cytometry. Anal Biochem. 2012; 420:26–32. [PubMed: 21893022]

45. Ng DC, Lin BH, Lim CP, Huang G, Zhang T, Poli V, et al. Stat3 regulates microtubules by antagonizing the depolymerization activity of stathmin. J Cell Biol. 2006; 172:245–257. [PubMed: 16401721]

46. Jin L, Li D, Alesi GN, Fan J, Kang HB, Lu Z, et al. Glutamate dehydrogenase 1 signals through antioxidant glutathione peroxidase 1 to regulate redox homeostasis and tumor growth. Cancer Cell. 2015; 27:257–270. [PubMed: 25670081]

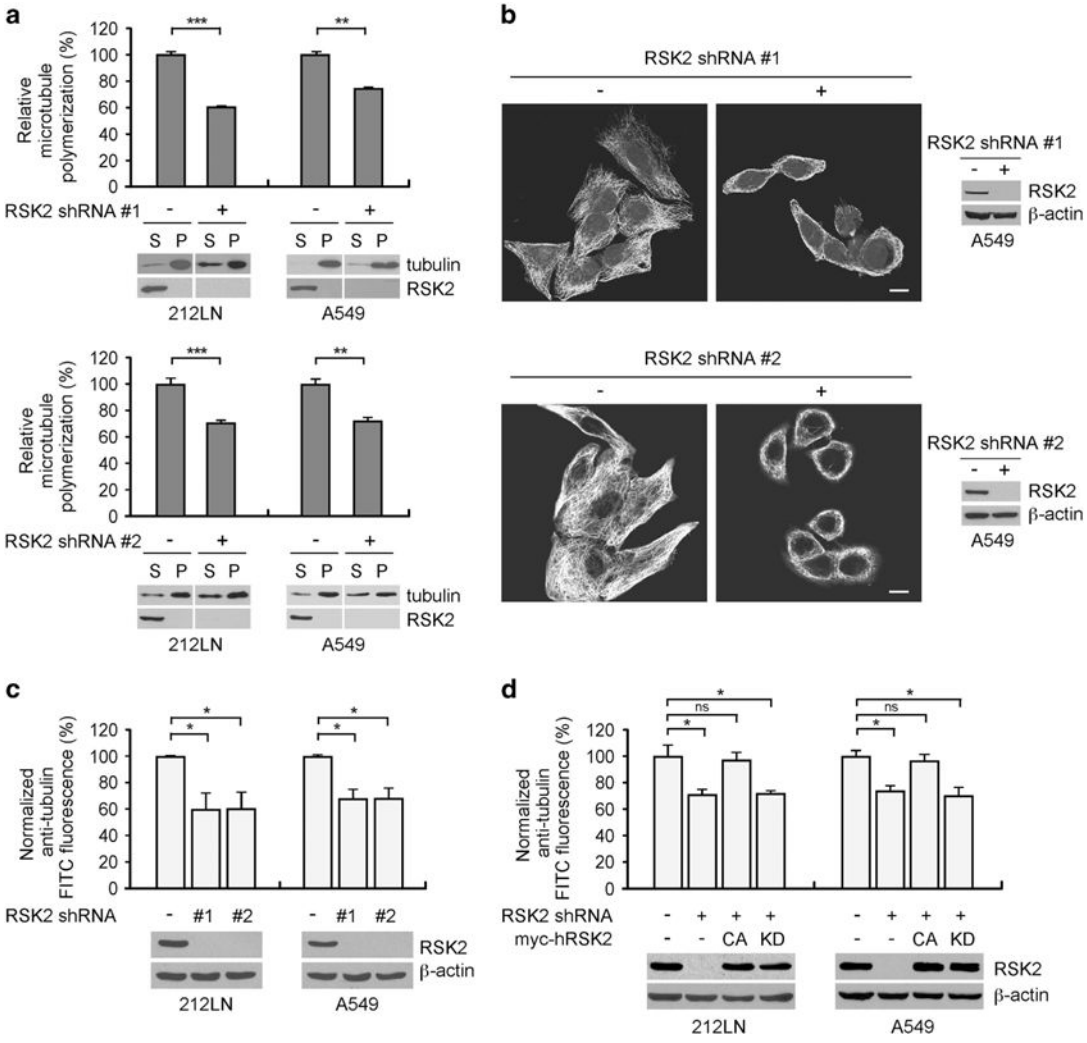

Figure 1.

Targeted downregulation of RSK2 attenuates microtubule polymerization in metastatic human cancer cells. (**a**) Tubulin sedimentation assay shows that RNAi-mediated stable knockdown of RSK2 results in significantly decreased microtubule polymerization in HNSCC 212LN cells (left) and lung cancer A549 cells (right). Lower: Tubulin immunoblots show soluble and polymerized tubulin in the supernatant (S) and pellet (P), respectively. Upper: Relative tubulin polymerization was determined by density analysis. The amount of polymerized tubulin in cells with RSK2 knockdown was normalized to the tubulin polymerization of control cells with an empty vector. (**b**) Tubulin immunofluorescence staining shows that stable knockdown of RSK2 disrupts tubulin polymerization in 212LN cells. Scale bar represents 10 μm. Western blotting shows RSK2 knockdown. (**c**) Polymerized tubulin was quantified by FACS-based whole-cell analysis of microtubules in RSK2 knockdown cells. FITC fluorescence intensity was normalized to a value of 100 for the control cells harboring an empty vector. (**d**) FACS-based whole-cell microtubule analysis using RSK2 knockdown cells with overexpression of shRNA-resistant CA (Y707A) or KD (Y707A/K100A) human RSK2. Stable RSK2 knockdown cells were transiently transfected with Y707A or Y707A/K100A RSK2 cDNA prior to microtubule analysis. Data represent

mean ± s.d. from three technical replicates. Results of one representative experiment from at least two independent experiments are shown. Statistical significance was determined using two-tailed Student's *t*-test (NS: not significant; *0.01<*P*<0.05; **0.001<*P*<0.01; ***$P<0.001$).

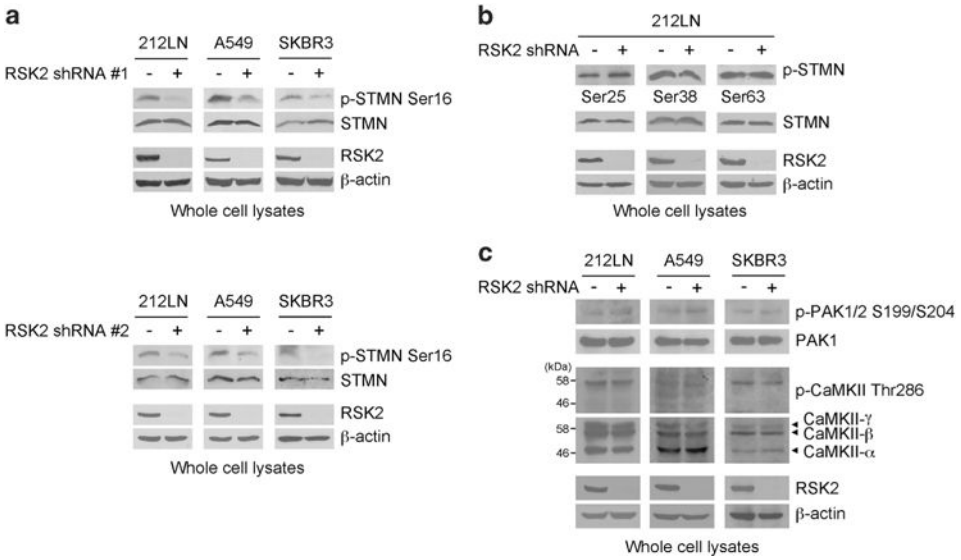

Figure 2.

RSK2 promotes stathmin phosphorylation in diverse metastatic cancer cells. (**a** and **b**) Effect of RSK2 stable knockdown on stathmin (STMN) phosphorylation at N-terminal serine residues, S16 (**a**), S25, S38 and S68 (**b**) in metastatic human cancer cells, 212LN, A549 and SKBR3. RSK2 knockdown using two different shRNA clones attenuates phosphorylation at stathmin S16 (**a**). (**c**) RSK2 knockdown effect on the activity of CaMKII and PAK1, known upstream kinases of stathmin. Activities of PAK1 and CaMKII were assessed by autophosphorylation at S199/S204 and T286, respectively, in diverse metastatic human cancer cells with RSK2 stable knockdown and control vector cells. SKBR3 cells were stimulated with 0.5 M sorbitol for phospho-PAK1 detection. Results of one representative experiment from at least two independent experiments are shown.

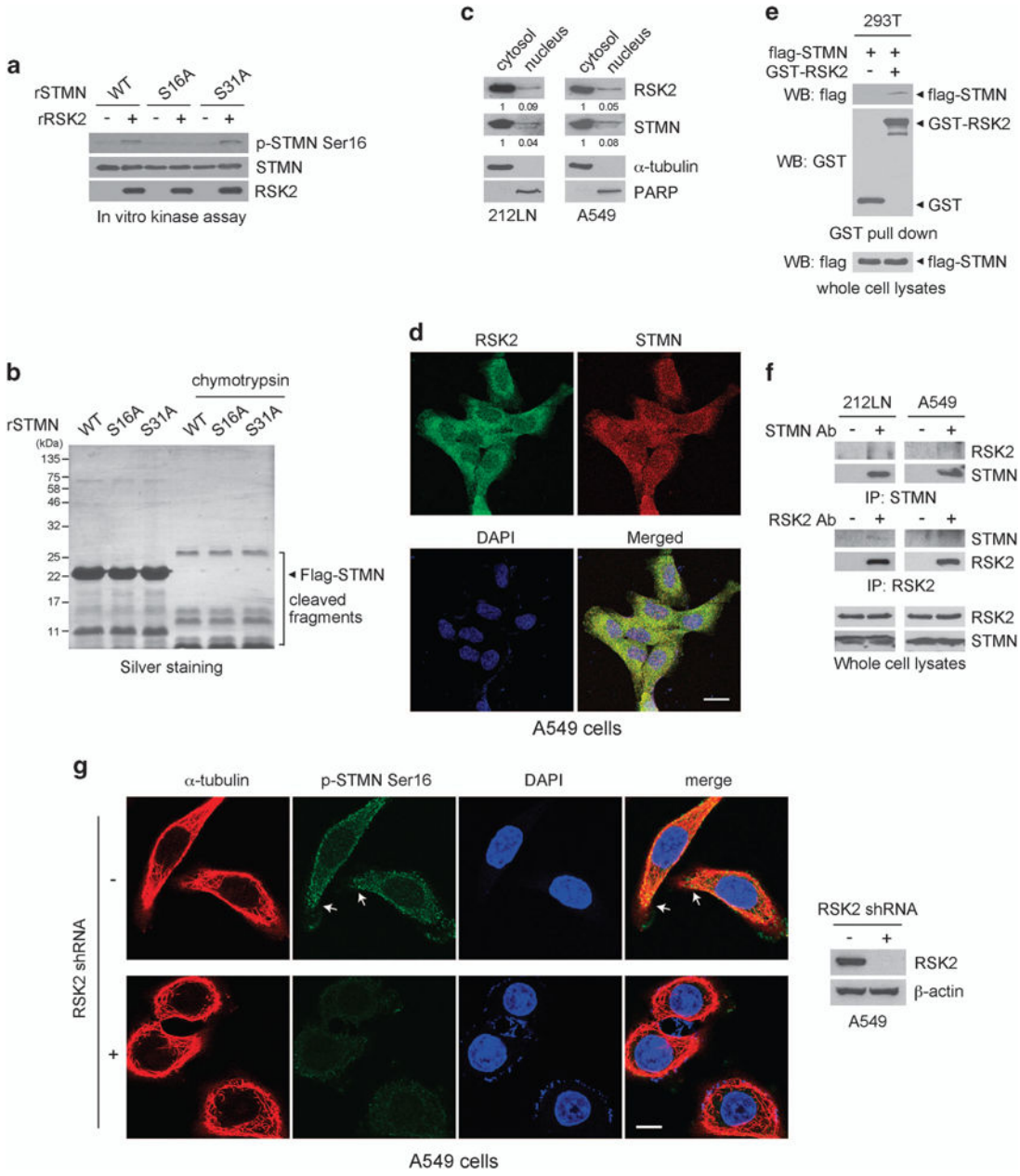

Figure 3.

RSK2 directly phosphorylates and interacts with stathmin in cells. (**a**) RSK2 directly phosphorylates stathmin (STMN) at S16. Purified recombinant stathmin (rSTMN) variants, WT, S16A and S31A, were incubated with recombinant active RSK2. Phosphorylation at serine 16 of stathmin was detected by western blotting using specific antibody against phospho-stathmin at S16. (**b**) Partial protease digestion demonstrates that the global structure of stathmin is not changed by point mutations. In all, 0.5 units of chymotrypsin were incubated with recombinant stathmin variants at 30 °C for 30 min and the digestion patterns were compared. (**c**) Western blots show the cytosolic/nuclear localization of RSK2 and stathmin in cancer cells. α-Tubulin and PARP (poly ADP-ribose polymerase) were used as control markers for cytosol and nucleus, respectively. (**d**) Immunofluorescence assay of

RSK2 and stathmin in A549 cells. Scale bar represents 20 μm. (**e**) RSK2 interacts with stathmin. GST or GST-fused RSK2 were enriched by GST pull-down assay from 293T cells transfected with flag-tagged stathmin. Stathmin in the complex of bead-bound GST-RSK2 was detected by western blotting. (**f**) Co-immunoprecipitation of endogenous RSK2 and stathmin in 212LN and A549 cells. (**g**) Immunofluorescence assay shows the localization of phosphorylated form of stathmin and tubulin in A549 cells with or without RSK2 shRNA. Scale bar represents 10 μm. Results of one representative experiment from at least two independent experiments are shown.

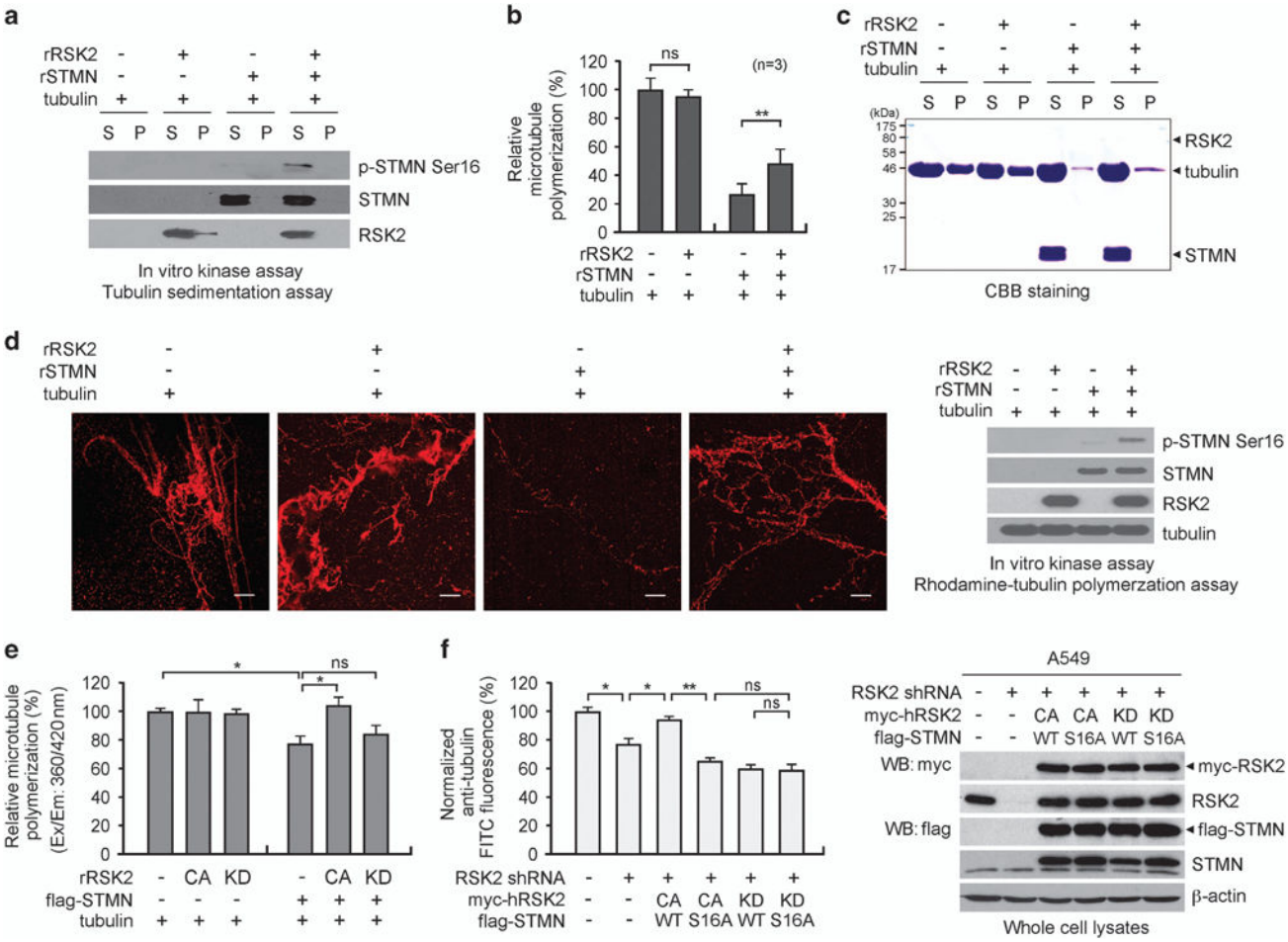

Figure 4.

RSK2-dependent phosphorylation of stathmin promotes microtubule polymerization. Purified stathmin (STMN) was phosphorylated via an *in vitro* RSK2 kinase assay and incubated with tubulin. (**a**) Stathmin phosphorylation in supernatant and pellet fractions is shown by western blotting analysis. (**b** and **c**) Polymerized tubulin was analyzed by Coomassie blue staining. S: supernatant, P: pellet. Relative tubulin polymerization in the absence or presence of RSK2 and/or stathmin was quantified by analyzing three independent repeats of microtubule polymerization assays (**b**). Representative image is shown panel (**c**). (**d**) Rhodamine-labeled tubulin was polymerized with stathmin alone or with stathmin preincubated with RSK2 and analyzed by fluorescence microscopy. Scale bars represent 30 μm. (**e**) Tubulin polymerization in the presence of recombinant stathmin, active RSK2 (CA) or inactive RSK2 (KD) in the indicated combination. Polymerized tubulin was quantified using the Fluorimetry-based Tubulin Polymerization Assay Kit. (**f**) FACS-based whole cell microtubule analysis of RSK2 knockdown cells overexpressing shRNA-resistant CA or KD RSK2 along with WT or S16A stathmin. Stable RSK2 knockdown cells were transiently transfected with distinct RSK2 and stathmin variants prior to whole-cell microtubule analysis. Results of one representative experiment from at least two independent experiments are shown. Data represent mean ± s.d. Statistical significance was determined using two-tailed Student's *t*-test (NS: not significant; *0.01<*P*<0.05; **0.001<*P*<0.01).

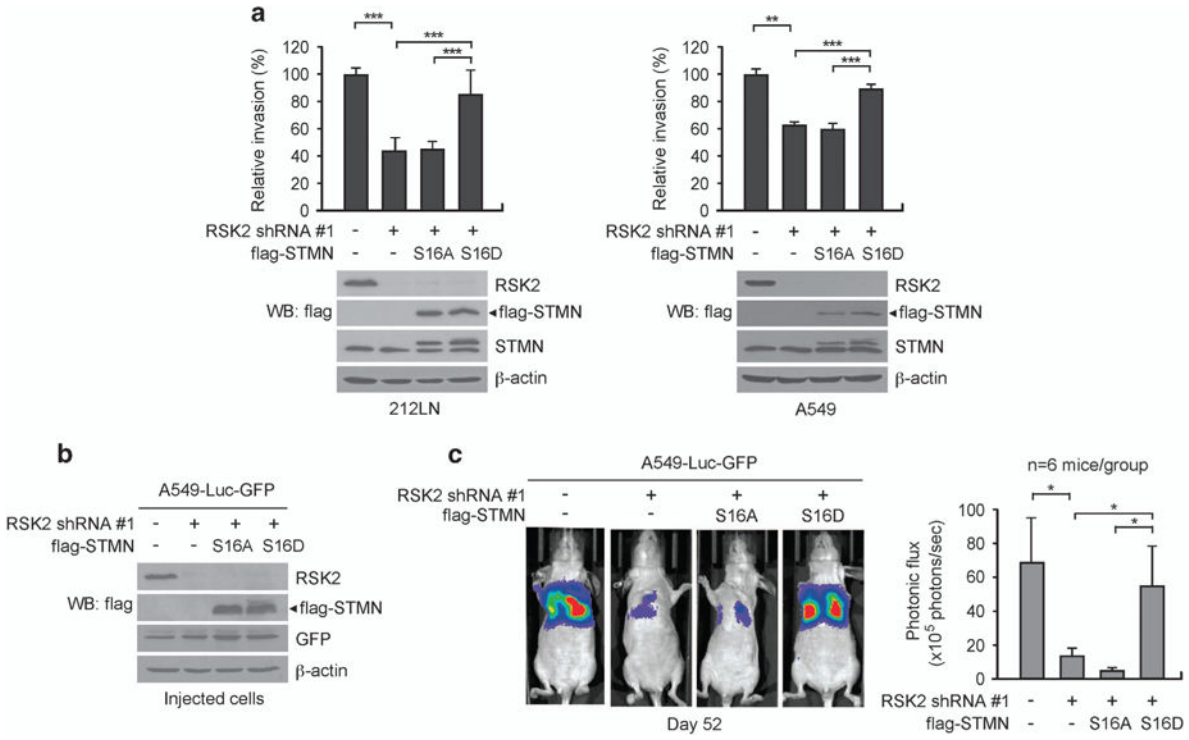

Figure 5.

RSK2 promotes cancer cell invasion and tumor metastasis, in part, through phosphorylation of stathmin. (**a**) Matrigel invasion assay using RSK2 knockdown cells with stathmin (STMN) variants. Stable expression of phospho-mimetic mutant S16D stathmin but not phospho-deficient mutant S16A stathmin restored the cancer cell invasion attenuated by RSK2 knockdown in 212LN and A549 cells. (**b**) RSK2, flag-tagged stathmin S16A and S16D expression was detected by immunoblotting in A549-luc-GFP cells used for tail-vein injection. (**c**) Left: BLI imaging of representative mice injected with A549-luc-GFP cells with RSK2 knockdown and S16A or S16D stathmin expression at day 52 after injection. Right: Average photonic flux of each group at weeks 6–8 is shown. (**a**) Data represent mean ± s.d. from nine (left) and four (right) technical replicates. Results of one representative experiment from at least two independent experiments are shown. (**c**) Data represent mean ± s.e.m. from six mice for each group. Statistical significance was determined using two-tailed Student's *t*-test for panel (**a**) and one-tailed Student's *t*-test for panel (**c**) (*0.01<*P*<0.05; **0.001<*P*<0.01; ***$P<0.001$).

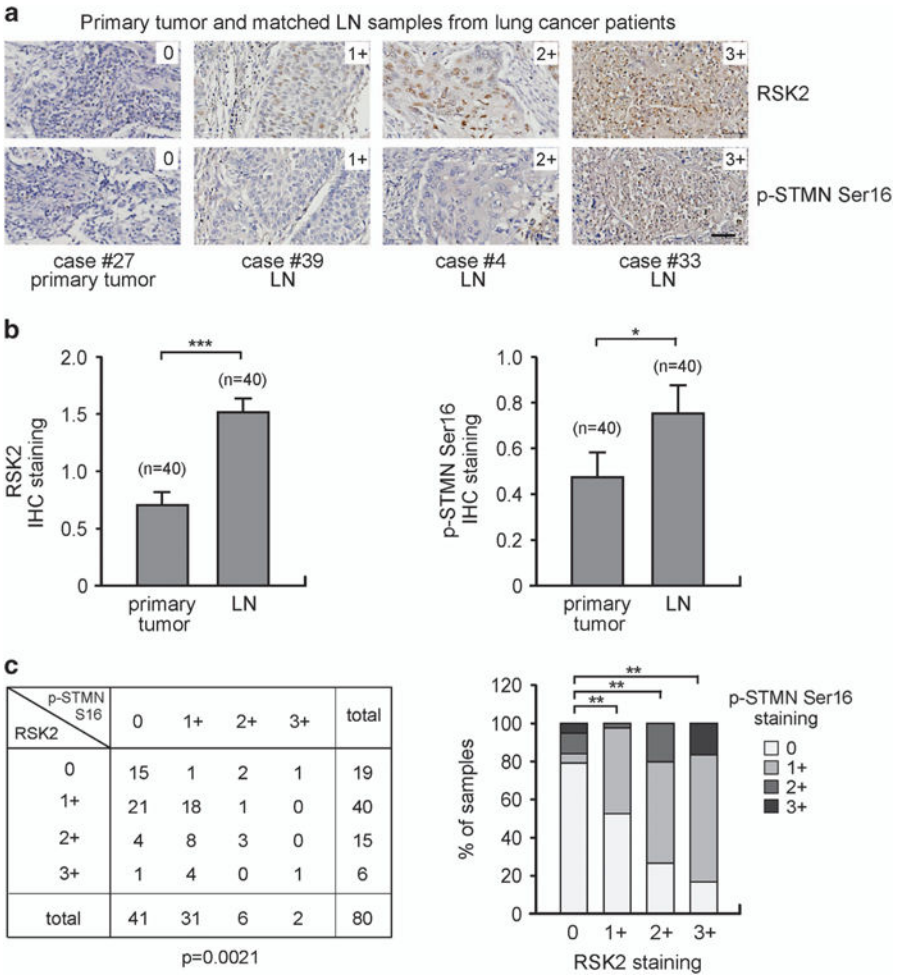

RSK2 \ p-STMN S16	0	1+	2+	3+	total
0	15	1	2	1	19
1+	21	18	1	0	40
2+	4	8	3	0	15
3+	1	4	0	1	6
total	41	31	6	2	80

Figure 6.

The levels of RSK2 and phospho-S16 stathmin correlate with metastatic cancer progression in primary human tumor tissue samples from lung cancer patients. The levels of RSK2 and stathmin (STMN) phosphorylation in 40 cases of human lung cancer with matched lymph node (LN) metastasis were determined by IHC staining using lung cancer tissue microarray. (**a**) Representative tumor specimens with staining intensity of 0 (negative), 1+ (weak), 2+ (moderate) and 3+ (strong) of RSK2 and phospho-stathmin S16 are shown. Scale bar represents 50 μm. (**b**) Levels of RSK2 expression (left) and stathmin phosphorylation (right) in primary tumors and matched tumors from lymph nodes. The staining intensity was scored from 0 to 3+. Data represent mean ± s.e.m. from $n = 40$/group. (**c**) The correlation between RSK2 and phospho-stathmin S16 was determined. Bar graph representation is shown on the right. *P*-values were determined by two-tailed paired Student's *t*-test for panel (**b**) and chi-square test for panel (**c**) (*0.01<*P*<0.05; **0.001<*P*<0.01; ***$P<0.001$).